

Strain activation of localized states in WSe_2

Oğuzhan Yücel,* Denis Yagodkin, Jan N. Kirchhof, Abhijeet Kumar, Adrian Dewambrechies, Sviatoslav Kovalchuk, Yufeng Yu, and Kirill I. Bolotin*

Department of Physics, Freie Universität Berlin, Berlin

E-mail: oguzhan.yuecel@fu-berlin.de; kirill.bolotin@fu-berlin.de

Abstract

We explore strain-activated emission centers formed by atomic force microscopy (AFM) indentation in monolayer WSe_2 on a flexible polymer substrate. In the indented areas, we observe sharp new photoluminescence (PL) peaks characterized by sublinear power dependence in the spectral regions 1.62 – 1.66 eV and 1.70 – 1.73 eV. After low-temperature thermal annealing (< 120 °C), WSe_2 experiences strain relaxation, leading to a blue shift of the peaks' spectral position and their ultimate disappearance. Our analysis of peaks' position vs. strain allows drawing multiple conclusions regarding the nature of these emission centers. We elucidate the roles of excitonic confinement and hybridization between free excitons and defect-related states, a process activated by the level of strain. Overall, our approach suggests that the energy of localized emitters may be controlled via strain engineering.

Introduction

Two-dimensional semiconductors from the group of transition metal dichalcogenides (TMDs) support a diverse zoo of excitons with varying properties.¹⁻⁴ Earlier studies of the excitonic landscape focused on free excitons, such as neutral excitons, charged excitons, biexcitons, and other species, while viewing disorder-localized excitonic states⁵ as an unwanted artifact. More recently, localized excitonic states distinguished by their sublinear power dependence became a budding research topic in their own right.⁶ First, localized excitonic states have been found to “store” spin and valley information in TMDs.^{7,8} Second, localized states have been employed to create single photon emitters (SPEs) in TMDs.^{9,10} While the coherence or stability properties of such emitters are inferior compared to more established technologies, e.g. NV centers in diamond,¹¹ TMD SPEs are distinguished by their spatial position right at the surface of the material (so that they can be coupled to external objects, e.g. for sensing or enhancement), electrical tunability stemming from the semiconductor nature of the TMDs, and the variability of emission energy.^{12,13}

In general, it is well-established that SPEs appear in several materials from the TMD family, notably in WSe₂, under the application of inhomogeneous strain.^{14,15} Such strain fields can be applied by depositing TMDs onto the pre-patterned substrates^{14,15} or by indenting TMDs by sharp atomic force microscope (AFM) tips.^{10,16,17} The strain-induced SPEs are heralded by the appearance of sharp new peaks in photoluminescence spectra characterized by narrow spectral width and sublinear power dependence. Electrical control, energy-tunability, and coupling to dielectric and plasmonic antennas have been demonstrated for TMD SPEs.^{9,18-22}

Despite large recent interest in strain-related localized SPEs in TMDs and the ubiquity of approaches to produce them, their physical origins remain hotly debated.¹⁰ First, while some studies suggest that excitons are localized by strain-related potential, others suggest that otherwise “dark” defects activated in the presence of strain are required for emitters’ formation.²³⁻²⁵ It has also been suggested that local straining techniques can produce extrinsic

structural defects.^{14,15,26} Second, the role of strain-related exciton “funneling” in brightening the emitters remains debated.^{27–29} Finally, it is still unclear if the energy of the emitters can be controlled in a large spectral range, e.g. via variation of the strain magnitude.³⁰

Our work is devoted to answering some of these questions. We study strain-induced localized emitters by controllably indenting WSe₂ on top of a polymer substrate. We show that the strain induced in a specific emitter can be relaxed by thermal annealing. Next, we study changes in the emitter’s spectra vs. the amount of strain. Our data is consistent with emitters originating from hybridization between free excitons and defect states. Moreover, our results suggest a pathway toward spectrally manipulated SPEs.

Experimental setup: We induce the inhomogeneous strain by indenting a TMD on an elastic substrate by an AFM tip, following the approach of Ref.^{16,17} We start with Si/SiO₂ substrates covered with 300 nm of poly methyl-methacrylate polymer (PMMA). We then mechanically exfoliate monolayer WSe₂ onto these substrates. We indent these samples under the application of a controlled force (Fig. S2), around 5 – 5.5 μN , positioning the AFM tip over a rectangular array of markers. The force values roughly exceeding 5.5 μN result in damage to the flake, whereas force values below 4.5 μN fail to consistently produce a well-defined indentation profile. Additional markings on the sample allow us to identify the same region of the sample during successive optical measurements (Fig. 1a). In general, the applied force of 5 μN results in a ~ 40 nm deep indentation with lateral dimensions on the scale of 200 nm (Fig. 1b). We only indent and analyze flat smooth sample regions without cracks or wrinkles to avoid artifacts in our analysis.

Next, we record changes in photoluminescence (PL) spectra from the same sample placed in an optical cryostat before and after indentation at $T = 6$ K. We use an excitation laser with 532 nm wavelength at varying power $P = 10$ nW – 10 μW to resolve localized features. The spatially localized emission character is shown in Fig. S1. Before the indentation (Fig. 1c, black), we observe excitonic features routinely seen in WSe₂ monolayers – a neutral exciton (X_0) at 1.75 eV and features typically associated with other excitonic states and disorder

below 1.7 eV.^{1,31} We observe the appearance of new features after the indentation in more than half of all measured indented regions. These peaks generally emerge at device-specific energies below 1.75 eV. In a representative sample, for instance, we observe two new features at 1.718 eV and 1.670 eV (Fig. 1c, red).

These new peaks have several key characteristic traits.^{32,33} First, the peaks are sharp, e.g., full width at half maximum (FWHM) of 1.3 meV for the peak at 1.718 eV in Fig. 1c, smaller than that for other free and disorder-related excitons (e.g., FWHM=13 meV for X_0). Second, the PL intensity (I_{PL}) exhibits sublinear power (P) dependence, $I_{PL} \approx P^\alpha$, with α between 0.5 – 0.7, consistent with previous studies of indented samples^{24,34} (Fig. 1d). Third, the peak is only visible at low temperatures and disappears when $T > 30$ K. All of these features have been previously observed in locally strained samples by multiple groups, and explained in the context of strain-induced localized states exhibiting single-photon emitter behavior.^{30,35–37} We therefore conclude that our AFM indentation approach also generates strain-related localized states.

While the emission from the indented region is stable over days, we noticed pronounced changes over longer time scales. After two months of storage at ambient conditions, we observed that indentation-related peaks in three representative indented regions, originally around 1.645 eV, shifted to higher energy, around 1.715 eV, and disappeared in some cases (Fig. 2b, green trace). These changes are concomitant with the reduction of the indentation depth, e.g., from 33 nm to 27 nm for an indentation in Fig. 2a. Such changes suggest the glassy flow of the PMMA polymer accompanied by strain relaxation. Such a flow should be dramatically accelerated at elevated temperatures. Indeed, after a subsequent brief (5 minutes) heating to 120 °C, the indentation depth of the same device in Fig. 2a reduced from 27 nm to 19 nm, while the indentation-related peaks disappeared almost completely in all three emission centers (Fig. 2b, blue trace).

We now systematically show that the post-indentation changes are indicative of strain relaxation induced by the thermal treatment of the device. It is necessary to analyze multiple

indented regions since strain-related peaks arise at varying energies in different devices and every emitting region has a different geometrical shape. We, therefore, analyze 25 indented points following the indentation and after annealing at 60 °C (we used lower temperature to avoid the complete disappearance of the emitters). The subsequent PL measurements are carried out, as before, at cryogenic temperature. It is worth noting that the changes we observe cannot be explained simply by the modified charge state of the sample, since all indentation-related peaks are much narrower compared to commonly observed charged excitons.

First, we systematically analyze changes in average strain, $\varepsilon_{avg} \equiv \langle \varepsilon_{xx} \rangle + \langle \varepsilon_{yy} \rangle$ before and after annealing (averaging over the entire indentation area). We estimate $\varepsilon_{avg} \approx (A - A_{projected})/A$, where A is the geometric area of the indentation region determined by the analysis of the rectangular-shaped (310 nm \times 380 nm) area of the AFM image centered on the indentation spot, and $A_{projected}$ is the area of the same rectangular region projected onto the xy plane.³⁸ In general, the strain determined from this expression is given by the average strain in the rectangular region surrounding the indentation spot. The distribution of ε_{avg} directly after the indentation is shown in Fig. 3a, red histogram; the ensemble (set of all measured spots) average strain is $2.5 \pm 0.5\%$. For the samples subjected to annealing at 60°C, the ensemble-averaged (over all indented regions) strain decreased to $\varepsilon_{avg} = 0.7 \pm 0.2\%$ (Fig. 3a). This is consistent with our observations from Fig. 2.

Next, we analyze the statistical changes in the PL spectra before and after annealing (Fig. 3b). To visualize indentation-related peaks in many regions, we chose to represent the PL peaks by their amplitudes η , evaluated as the area under the corresponding peak (obtained from a Gaussian fit to the data) normalized by its FWHM. To exclude free-excitonic features, we only analyze the peaks with FWHM twice smaller than that for free excitons. To facilitate the comparison of various peaks across different spectra, we perform a spectral shift and alignment procedure, ensuring that all spectra X_0 were adjusted to the same reference X_0 position at 1.750 eV. In general, peaks with large η correspond to intense

and narrow features. In Fig. 3b, we plotted the amplitudes η of all peaks in the 25 spots before and after indentation, as well as after annealing. These results confirm the behavior already seen in the representative device in Fig. 2b (panel on the right). Before indentation, we see the majority of excitonic peaks in the region 1.66 – 1.7 eV (white region). These peaks not caused by indentation are likely related to preexisting structural defects and/or localized strain and this spectral region, therefore, are not analyzed further. Directly after the indentation, we predominantly observe new intense peaks in the region <1.66 eV (yellow-shaded region). After the annealing, the number of peaks in the region <1.66 eV sharply drops, whereas some sharp features emerge in the region >1.70 eV.

These observations allow us to draw several conclusions regarding the nature of strain-induced localized peaks. First, the character of localized emitters is not consistent with a commonly assumed model – free excitons confined by the localized potential near the strain maximum in the indented region. Indeed, if that were the case, we would expect the PL emission at the energy $E = E_{free} - \varepsilon_{max} \times 47 \text{ meV}/\%$, where $E_{free} = 1.75$ eV is the energy of free excitons, ε_{max} is the maximum strain, and $47 \text{ meV}/\%$ is the amount of redshift of the excitons with applied uniaxial strain.³⁹ Since $\varepsilon_{max} \gg \varepsilon_{avg} \sim 2\%$, we expect the emission at energies below $\ll 1.65$ eV, much smaller compared to the observed energy range (Fig. S3). In contrast, our observations are consistent with normally dark structural defects brightening under strain through hybridization with free excitons.^{7,10,27,40} Our data suggest that there are several different types of structural defects which can all couple to free excitons depending on the amount of strain. Indeed, when the strain is large, we see sharp peaks predominantly in the region 1.62 – 1.66 eV, and in the region 1.70 – 1.73 eV for lower strain, hinting that different emitter types are “responsible” for these regions. Third, while our indentation approach can result in the coupling of free excitons to the structural defects already present in the material, it does not produce new defects or nanoscale holes. This conclusion is supported by the disappearance or near-disappearance of localized peaks after strain relaxation (Fig. 2b). Finally, we propose that strain-related funneling is at least

partially responsible for the high brightness of the localized emitters. Indeed, we observe brighter emission from the emitters in high-strain devices (red points in Fig. 3b).

To summarize, we investigated statistical changes in strain-induced localized emitters in indented monolayer WSe₂. We found that the average strain state of emitters can be tuned by heating the device. By analyzing changes in the optical spectra of individual emitters vs. strain, we can draw several conclusions regarding the emitter's character. In particular, our data is consistent with several different types of structural emitters being hybridized with free excitons depending on the strain state. Moreover, we excluded the role of extrinsic structural defects caused by indentation. Finally, our approach suggests that the energy of localized states may be controlled via strain engineering. This capability may prove useful in quantum technologies. At the same time, gradual strain relaxation in PMMA-based samples suggests that different types of elastic materials may be needed to enable functional indentation-based devices.

Acknowledgement

The authors thank Bianca Höfer for facility management. We acknowledge financial support through BMBF, German Federal Ministry for Education and Research, project 05K22KE3, and DFG, German Research Foundation, Project ID: 449596295 and TRR227 B08, 328545488.

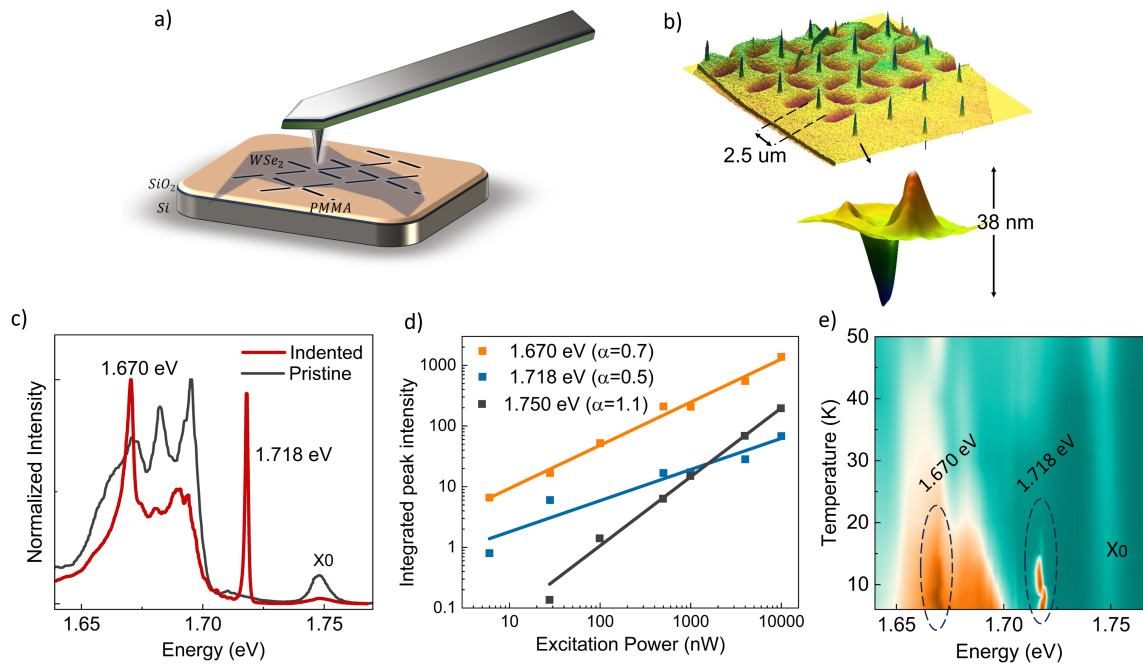


Figure 1: **Creation of position-controllable localized emission centers in WSe_2/PMMA** a) Cartoon of the setup. A WSe_2/PMMA sample is locally indented by an AFM tip, b) AFM images of the indented sample, c) Photoluminescence spectra at $T=6\text{K}$ from the same sample point before (black) and after (red) indentation. New sharp PL peaks 1.670 eV and 1.718 eV appearing after indentation are prominent. d), e) Power and temperature dependencies of the peaks at 1.670 eV and 1.718 eV, respectively, are consistent with their localized character.

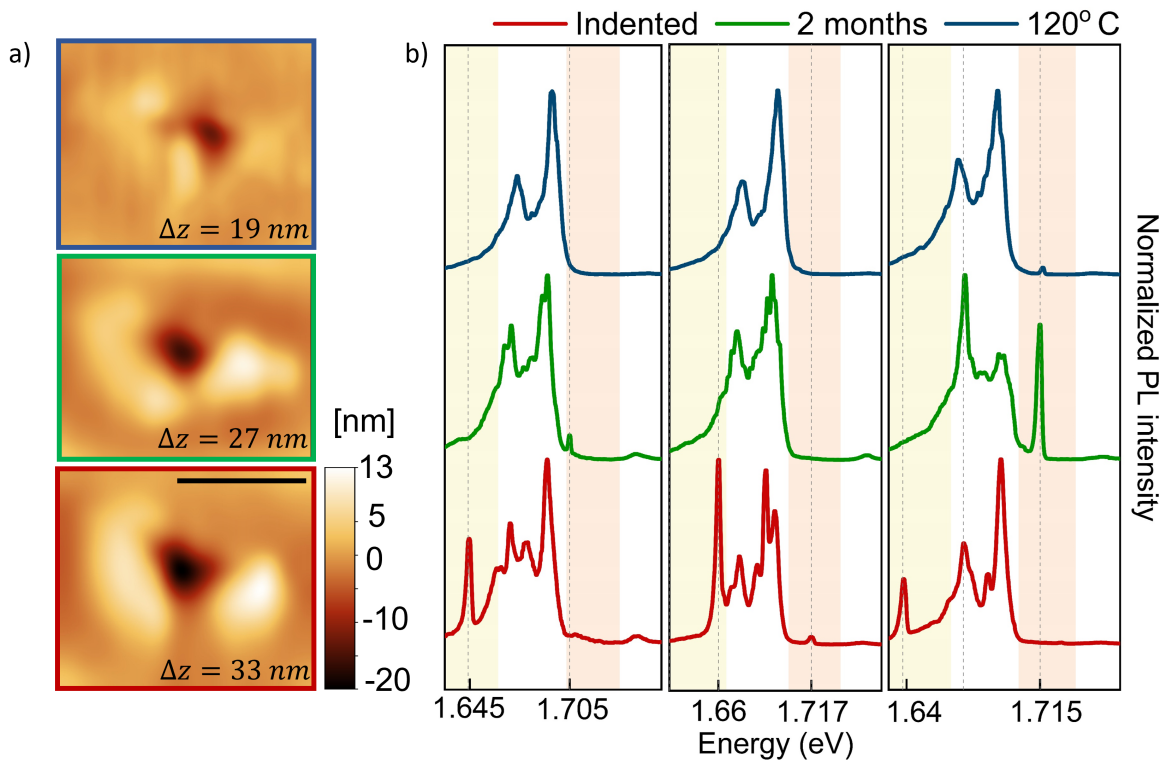


Figure 2: **Controlling the strain state of the sample via annealing.** AFM images at the same region (a) (The scale bar is 200 nm) and PL spectra of three representative emitters (b) after indentation (red), two months later at ambient condition (green), and after subsequent 5 min annealing at 120°C (blue). Strain relaxation after each step is apparent in a). Indentation-related peaks appearing inside the shaded regions and blue-shifting at each stage of the process are seen in b).

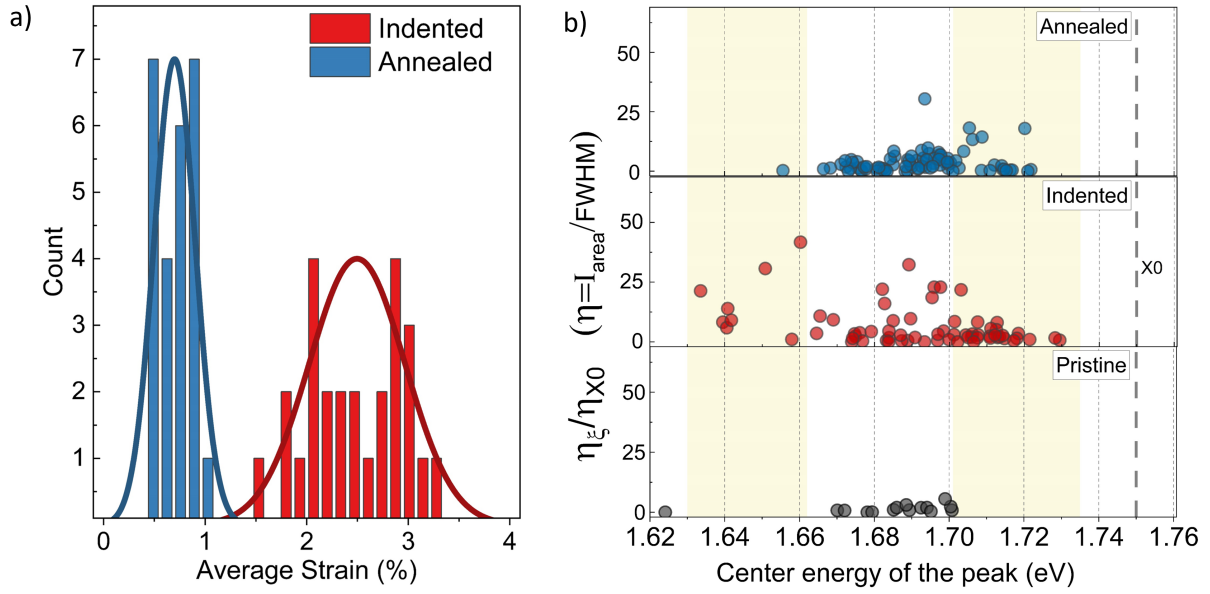


Figure 3: **Evolution of PL during strain relaxation** a) A histogram of average strain in 25 indentation areas before and after temperature cycling to 60 °C. A reduction of strain after annealing is apparent. b) Histograms of peaks “heights” (defined as area under the peak/FWHM) vs. peak central energy for all 25 areas before and after the indentation, as well as after temperature cycling. To compare to spectra from different devices and account for substrate-wide doping and strain variations, each spectrum is aligned according to $X_0 = 1.750$ eV and normalized by their own intensity of corresponding X_0 peak.

References

- (1) Wang, G.; Chernikov, A.; Glazov, M. M.; Heinz, T. F.; Marie, X.; Amand, T.; Urbaszek, B. Colloquium: Excitons in atomically thin transition metal dichalcogenides. *Reviews of Modern Physics* **2018**, *90*, 021001.
- (2) Regan, E. C.; Wang, D.; Paik, E. Y.; Zeng, Y.; Zhang, L.; Zhu, J.; MacDonald, A. H.; Deng, H.; Wang, F. Emerging exciton physics in transition metal dichalcogenide heterobilayers. *Nature Reviews Materials* **2022**, *7*, 778–795.
- (3) Mueller, T.; Malic, E. Exciton physics and device application of two-dimensional transition metal dichalcogenide semiconductors. *npj 2D Materials and Applications* **2018**, *2*, 29.
- (4) Berkelbach, T. C.; Hybertsen, M. S.; Reichman, D. R. Theory of neutral and charged excitons in monolayer transition metal dichalcogenides. *Physical Review B* **2013**, *88*, 045318.
- (5) Hoffmann, K. H.; Schreiber, M.; Runge, E. Randomness in Optical Spectra of Semiconductor Nanostructures. *Computational Statistical Physics: From Billiards to Monte Carlo* **2002**, 241–257.
- (6) Von der Osten, W.; Stolz, H. Localized exciton states in silver halides. *Journal of Physics and Chemistry of Solids* **1990**, *51*, 765–791.
- (7) Linhart, L.; Paur, M.; Smejkal, V.; Burgdörfer, J.; Mueller, T.; Libisch, F. Localized Intervalley Defect Excitons as Single-Photon Emitters in WSe₂. *Phys. Rev. Lett.* **2019**, *123*, 146401.
- (8) Wang, Y.; Deng, L.; Wei, Q.; Wan, Y.; Liu, Z.; Lu, X.; Li, Y.; Bi, L.; Zhang, L.; Lu, H.; others Spin-valley locking effect in defect states of monolayer MoS₂. *Nano letters* **2020**, *20*, 2129–2136.

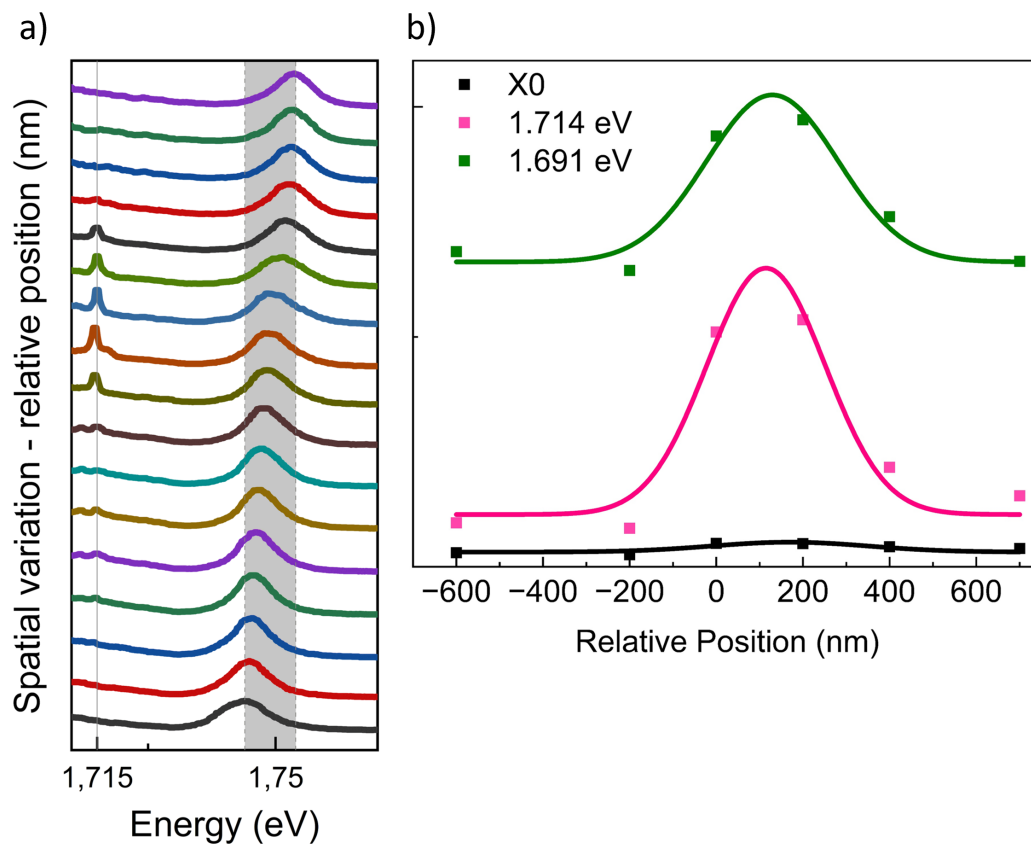
- (9) Palacios-Berraquero, C.; Palacios-Berraquero, C. Atomically-thin quantum light emitting diodes. *Quantum confined excitons in 2-dimensional materials* **2018**, 71–89.
- (10) Abramov, A. N.; Chestnov, I. Y.; Alimova, E. S.; Ivanova, T.; Mukhin, I. S.; Krizhanovskii, D. N.; Shelykh, I. A.; Iorsh, I. V.; Kravtsov, V. Photoluminescence imaging of single photon emitters within nanoscale strain profiles in monolayer WSe₂. *arXiv preprint arXiv:2301.09478* **2023**,
- (11) Jelezko, F.; Tietz, C.; Gruber, A.; Popa, I.; Nizovtsev, A.; Kilin, S.; Wrachtrup, J. Spectroscopy of Single N-V Centers in Diamond. *Single Molecules* **2001**, *2*, 255–260.
- (12) Wang, K.; De Greve, K.; Jauregui, L. A.; Sushko, A.; High, A.; Zhou, Y.; Scuri, G.; Taniguchi, T.; Watanabe, K.; Lukin, M. D.; others Electrical control of charged carriers and excitons in atomically thin materials. *Nature nanotechnology* **2018**, *13*, 128–132.
- (13) Zheng, W.; Jiang, Y.; Hu, X.; Li, H.; Zeng, Z.; Wang, X.; Pan, A. Light emission properties of 2D transition metal dichalcogenides: fundamentals and applications. *Advanced Optical Materials* **2018**, *6*, 1800420.
- (14) Palacios-Berraquero, C.; Kara, D. M.; Montblanch, A. R.-P.; Barbone, M.; Latawiec, P.; Yoon, D.; Ott, A. K.; Loncar, M.; Ferrari, A. C.; Atatüre, M. Large-scale quantum-emitter arrays in atomically thin semiconductors. *Nature communications* **2017**, *8*, 15093.
- (15) Branny, A.; Kumar, S.; Proux, R.; Gerardot, B. D. Deterministic strain-induced arrays of quantum emitters in a two-dimensional semiconductor. *Nature communications* **2017**, *8*, 15053.
- (16) Rosenberger, M. R.; Dass, C. K.; Chuang, H.-J.; Sivaram, S. V.; McCreary, K. M.; Hendrickson, J. R.; Jonker, B. T. Quantum calligraphy: writing single-photon emitters in a two-dimensional materials platform. *ACS nano* **2019**, *13*, 904–912.

- (17) So, J.-P.; Kim, H.-R.; Baek, H.; Jeong, K.-Y.; Lee, H.-C.; Huh, W.; Kim, Y. S.; Watanabe, K.; Taniguchi, T.; Kim, J.; others Electrically driven strain-induced deterministic single-photon emitters in a van der Waals heterostructure. *Science Advances* **2021**, *7*, eabj3176.
- (18) Azzam, S. I.; Parto, K.; Moody, G. Purcell enhancement and polarization control of single-photon emitters in monolayer WSe₂ using dielectric nanoantennas. *Nanophotonics* **2023**, *12*, 477–484.
- (19) Patel, S. D.; Parto, K.; Choquer, M.; Umezawa, S.; Hellman, L.; Polishchuk, D.; Moody, G. Cavity Optomechanics with WSe₂ Single Photon Emitters. CLEO 2023. 2023; p FW3J.2.
- (20) Aharonovich, I.; Englund, D.; Toth, M. Solid-state single-photon emitters. *Nature Photonics* **2016**, *10*, 631–641.
- (21) Clark, G.; Schaibley, J. R.; Ross, J.; Taniguchi, T.; Watanabe, K.; Hendrickson, J. R.; Mou, S.; Yao, W.; Xu, X. Single defect light-emitting diode in a van der Waals heterostructure. *Nano letters* **2016**, *16*, 3944–3948.
- (22) Peng, L.; Chan, H.; Choo, P.; Odom, T. W.; Sankaranarayanan, S. K. R. S.; Ma, X. Creation of Single-Photon Emitters in WSe₂ Monolayers Using Nanometer-Sized Gold Tips. *Nano Letters* **2020**, *20*, 5866–5872.
- (23) Tongay, S.; Suh, J.; Ataca, C.; Fan, W.; Luce, A.; Kang, J. S.; Liu, J.; Ko, C.; Raghunathan, R.; Zhou, J.; others Defects activated photoluminescence in two-dimensional semiconductors: interplay between bound, charged and free excitons. *Scientific reports* **2013**, *3*, 2657.
- (24) Srivastava, A.; Sidler, M.; Allain, A. V.; Lembke, D. S.; Kis, A.; Imamoglu, A. Optically active quantum dots in monolayer WSe₂. *Nature Nanotechnology* **2015**, *10*, 491–496.

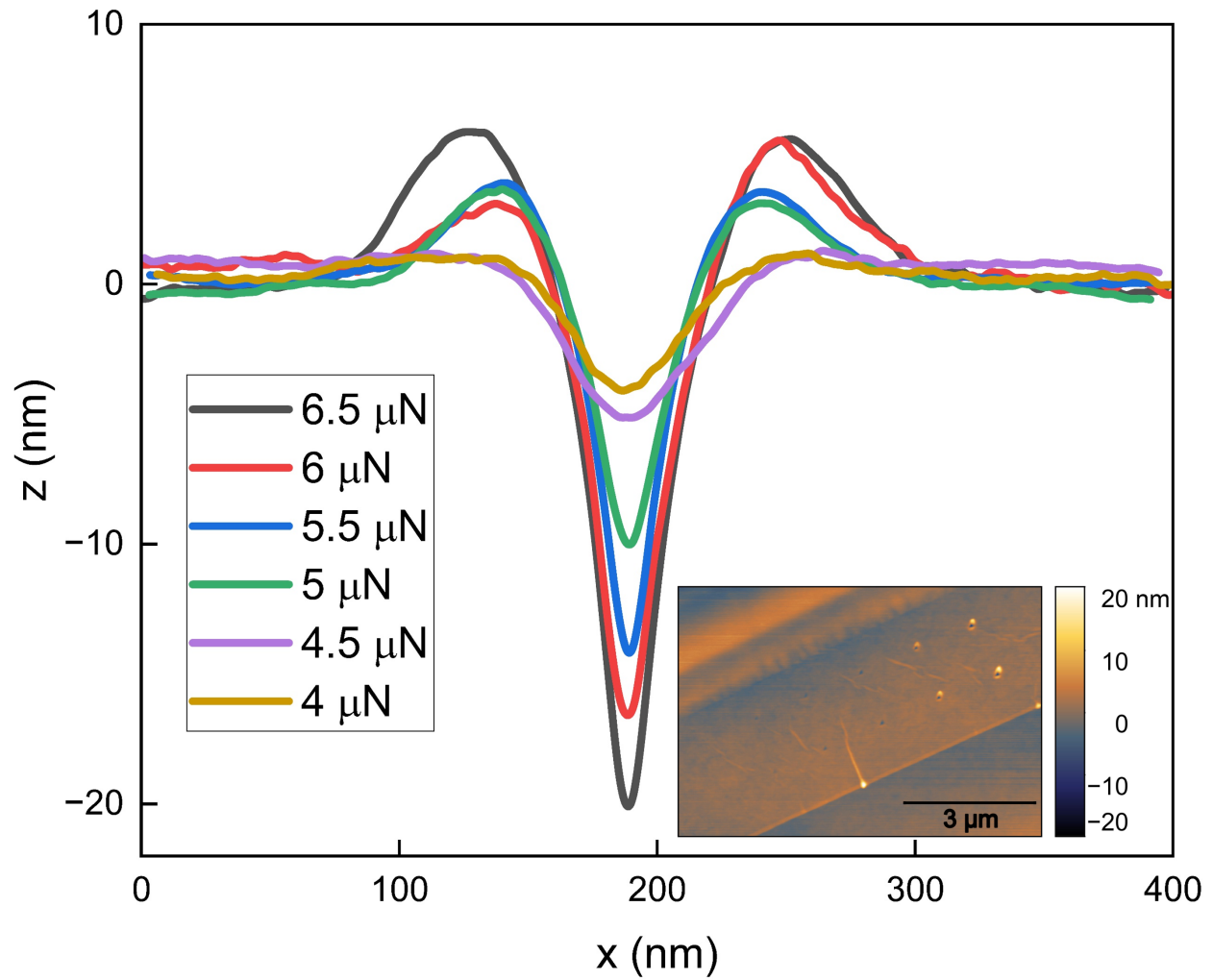
- (25) Chen, X.; Yue, X.; Zhang, L.; Xu, X.; Liu, F.; Feng, M.; Hu, Z.; Yan, Y.; Scheuer, J.; Fu, X. Activated Single Photon Emitters And Enhanced Deep-Level Emissions in Hexagonal Boron Nitride Strain Crystal. *Advanced Functional Materials* **2023**, 2306128.
- (26) Parto, K.; Azzam, S. I.; Banerjee, K.; Moody, G. Defect and strain engineering of monolayer WSe₂ enables site-controlled single-photon emission up to 150 K. *Nature Communications* **2021**, *12*, 3585.
- (27) Hernández López, P.; Heeg, S.; Schattauer, C.; Kovalchuk, S.; Kumar, A.; Bock, D. J.; Kirchhof, J. N.; Höfer, B.; Greben, K.; Yagodkin, D.; others Strain control of hybridization between dark and localized excitons in a 2D semiconductor. *Nature communications* **2022**, *13*, 7691.
- (28) Vutukuru, M.; Ardekani, H.; Chen, Z.; Wilmington, R. L.; Gundogdu, K.; Swan, A. K. Enhanced dielectric screening and photoluminescence from nanopillar-strained MoS₂ nanosheets: Implications for strain funneling in optoelectronic applications. *ACS Applied Nano Materials* **2021**, *4*, 8101–8107.
- (29) Harats, M. G.; Kirchhof, J. N.; Qiao, M.; Greben, K.; Bolotin, K. I. Dynamics and efficient conversion of excitons to trions in non-uniformly strained monolayer WS₂. *Nature Photonics* **2020**, *14*, 324–329.
- (30) Iff, O.; Tedeschi, D.; Martín-Sánchez, J.; Moczala-Dusanowska, M.; Tongay, S.; Yumigeta, K.; Taboada-Gutiérrez, J.; Savaresi, M.; Rastelli, A.; Alonso-González, P.; Höfling, S.; Trotta, R.; Schneider, C. Strain-Tunable Single Photon Sources in WSe₂ Monolayers. *Nano Letters* **2019**, *19*, 6931–6936.
- (31) Kirchhof, J. N.; Yu, Y.; Antheaume, G.; Gordeev, G.; Yagodkin, D.; Elliott, P.; De Araújo, D. B.; Sharma, S.; Reich, S.; Bolotin, K. I. Nanomechanical spectroscopy of 2d materials. *Nano letters* **2022**, *22*, 8037–8044.

- (32) Warburton, R. J.; Schäfflein, C.; Haft, D.; Bickel, F.; Lorke, A.; Karrai, K.; Garcia, J. M.; Schoenfeld, W.; Petroff, P. M. Optical emission from a charge-tunable quantum ring. *Nature* **2000**, *405*, 926–929.
- (33) Tran, T. T.; Bray, K.; Ford, M. J.; Toth, M.; Aharonovich, I. Quantum emission from hexagonal boron nitride monolayers. *Nature nanotechnology* **2016**, *11*, 37–41.
- (34) He, Y.-M.; Iff, O.; Lundt, N.; Baumann, V.; Davanco, M.; Srinivasan, K.; Höfling, S.; Schneider, C. Cascaded emission of single photons from the biexciton in monolayered WSe₂. *Nature Communications* **2016**, *7*, 13409.
- (35) Darlington, T. P.; Carmesin, C.; Florian, M.; Yanev, E.; Ajayi, O.; Ardelean, J.; Rhodes, D. A.; Ghiotto, A.; Krayev, A.; Watanabe, K.; others Imaging strain-localized excitons in nanoscale bubbles of monolayer WSe₂ at room temperature. *Nature Nanotechnology* **2020**, *15*, 854–860.
- (36) Kim, H.; Moon, J. S.; Noh, G.; Lee, J.; Kim, J.-H. Position and frequency control of strain-induced quantum emitters in WSe₂ monolayers. *Nano letters* **2019**, *19*, 7534–7539.
- (37) Aslan, B.; Deng, M.; Heinz, T. F. Strain tuning of excitons in monolayer WSe₂. *Physical Review B* **2018**, *98*, 115308.
- (38) Landau, L. D.; Lifshitz, E. M.; Kosevich, A. M.; Pitaevskii, L. P. *Theory of elasticity: volume 7*; Elsevier, 1986; Vol. 7.
- (39) Aslan, B.; Yule, C.; Yu, Y.; Lee, Y. J.; Heinz, T. F.; Cao, L.; Brongersma, M. L. Excitons in strained and suspended monolayer WSe₂. *2D Materials* **2021**, *9*, 015002.
- (40) Moon, H.; Bersin, E.; Chakraborty, C.; Lu, A.-Y.; Grosso, G.; Kong, J.; Englund, D. Strain-correlated localized exciton energy in atomically thin semiconductors. *ACS Photonics* **2020**, *7*, 1135–1140.

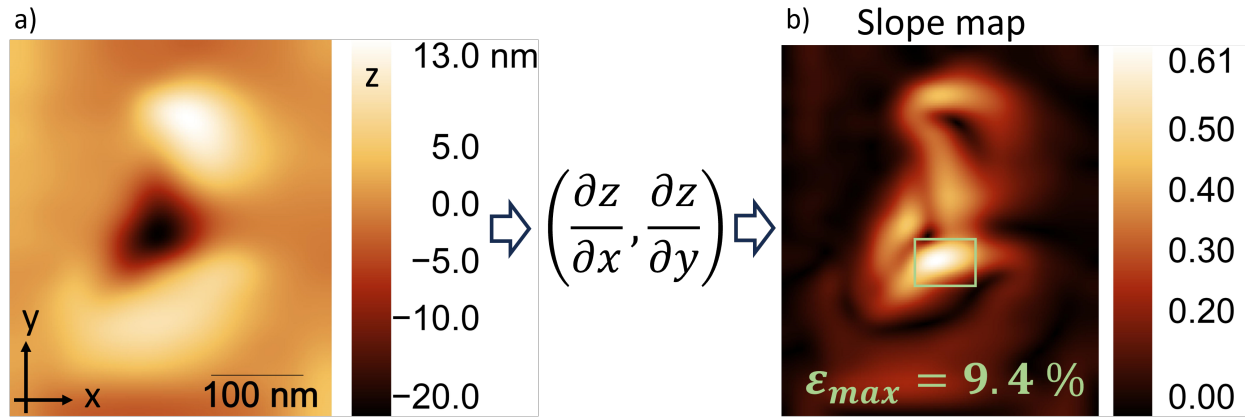
Supporting Information Available



Supplementary Figure 1: **Localized character of the emission.** a) PL intensity recorded at gradually changing spatial position across the indentation spot. The slight shift in the neutral exciton spectral position is due to prestress variation across the flake. b) The intensity of strain induced peaks (1.691, 1.714 eV) vs. spatial position.



Supplementary Figure 2: AFM topography of spots indented with force varying up to 6.5 μN .



Supplementary Figure 3: a) The AFM image of the sample in Fig. 2b (the spectra column at the right) b) Map of the slope magnitude, defined as $S = \sqrt{(\partial z/\partial x)^2 + (\partial z/\partial y)^2}$ for the exact same region indicating the stretching distribution across the indented flake. The area in the small frame in (b) where the slope vector reaches a maximum of 9.4%.